International Journal of Solids and Structures 48 (2011) 803–816

Contents lists available at ScienceDirect

International Journal of Solids and Structures

journal homepage: www.elsevier.com/locate/ijsolstr

Buckling and progressive crushing of laterally loaded honeycomb

A. Wilbert, W.-Y. Jang [1], S. Kyriakides *, J.F. Floccari

Research Center for Mechanics of Solids, Structures & Materials, The University of Texas at Austin, WRW 110, Austin, TX 78712, USA

ARTICLE INFO

Article history:
Received 3 August 2010
Received in revised form 20 October 2010
Available online 17 November 2010

Keywords:
Honeycomb
Buckling
Collapse
Crushing

ABSTRACT

This paper presents a comprehensive study of the lateral compressive response of hexagonal honeycomb panels from the initial elastic regime to a fully crushed state. Expanded aluminum alloy honeycomb panels with a cell size of 9.53 mm, a relative density of 0.026, and a height of 15.9 mm are laterally compressed quasi statically between rigid platens under displacement control. The cells buckle elastically and collapse at a higher stress due to inelastic action. Deformation then first localizes at mid-height and the cells crush by progressive formation of folds; associated with each fold family is a stress undulation. The response densifies when the whole panel height is consumed by folds. The buckling and crushing events are simulated numerically using finite element models involving periodic domains of a single or several characteristic cells. The models idealize the microstructure as hexagonal, with double walls in one direction. The nonlinear behavior is initiated by elastic buckling while inelastic collapse that leads to the localization observed in the experiments occurs at a significantly higher load. The collapse stress is found to be mildly sensitive to various problem imperfections. The subsequent folding can be reproduced numerically using periodic domains but requires a fine mesh capable of capturing the complexity of the folds. The calculated crushing response is shown to better resemble measured ones when a 4 × 4 cell domain is used. However, the average crushing stress can be captured with engineering accuracy even from a single cell domain.

1. Introduction

Honeycomb is a two-dimensional cellular material that is relatively strong and stiff along the normal to the microstructure but compliant and weak in-plane. It is widely used as core in sandwich construction where its role is to transfer shear loads between the faceplates (Allen, 1969, Marshall, 1982). Hexagonal cells are most common but circular, square and other cell geometries including ones that are auxetic and others that can accommodate bending of a sheet exist (Hexcel, 2010). Honeycomb is made from most materials, metals, polymers, paper, etc., to fit the application. Their wide use stems from their excellent specific stiffness and weight, their outstanding energy absorption characteristics and their cost effectiveness (Gibson and Ashby, 1997).

The wide use of honeycomb in practice generated a need for establishing their mechanical properties and this spawned an extensive literature on the subject starting from the anisotropic elastic properties, the onset of "yielding" and collapse, and the crushing response (e.g., Gibson and Ashby, 1997). Of all honeycombs, metallic ones with hexagonal cells have received the most attention. The extensive literature on the out of plane mechanical behavior was motivated first by the design needs of sandwich construction (e.g., Kelsey et al., 1958; Penzien and Didriksson, 1964; Grediac, 1993; Zhang and Ashby, 1992; Gibson and Ashby, 1997). The second motivation comes from the use of such honeycombs for energy absorption in a variety of quasi-static and dynamic applications (e.g., McFarland, 1963, 1964; Wierzbicki, 1983; Wierzbicki and Abramowicz, 1983; Goldsmith and Sackman, 1992; Mohr and Doyoyo, 2003, 2004a,b; Aktay et al., 2008; Yamashita and Gotoh, 2005; Zhao and Gary, 1998; Chen et al., 2009).

A similarly large literature on the in-plane properties is mainly motivated by the similarities between the behavior of three-dimensional cellular materials, namely foams, and that of honeycombs loaded and crushed in-plane; in other words, here the honeycomb represents a two-dimensional model for the more complex foams with space-filling three-dimensional microstructures (e.g., Gibson et al., 1982; Klintworth and Stronge, 1988; Papka and Kyriakides, 1994, 1998; Triantafyllidis and Schraad, 1998).

The present study is concerned with the more traditional problem of transverse compression. In particular, we aim to establish all aspects of the compressive response of honeycomb sandwich panels; that is, the initial linearly elastic behavior, the onset of instability, the onset of collapse, its localization, and the progressive folding and crushing under persistent compression. Of these properties, the crushing behavior, or in other words the energy

---

* Corresponding author.
E-mail address: skk@mail.utexas.edu (S. Kyriakides).

[1] Presently, Department of Mechanical Engineering, National Chiao Tung University, Hsinchu, Taiwan.

0020-7683/$ - see front matter © 2010 Elsevier Ltd. All rights reserved.
doi:10.1016/j.ijsolstr.2010.11.014

absorption capacity, has received the most attention experimentally (e.g., McFarland, 1963, 1964; Goldsmith and Sackman, 1992; Mohr and Doyoyo, 2004a) and analytically; early on using kinematically admissible collapse mechanisms (e.g., Wierzbicki, 1983; Wierzbicki and Abramowicz, 1983), and more recently more representative numerical models (e.g., Mohr and Doyoyo, 2004b; Yamashita and Gotoh, 2005 among others).

The study performed is based on a Hexcel Al alloy honeycomb bonded to Al faceplates. The honeycomb is manufactured as described in Papka and Kyriakides (1998) (see also Hexcel, 2010): lines of epoxy of chosen width and spacing are “printed” on thin metal foils. The foils are stacked together in a manner that places the bond lines of adjacent foils half a period out of phase as shown in Fig. 1a. The foil stacking is placed in a press with hot platens where the epoxy lines are cured. Axial strips of the required honeycomb thickness are then cut from the stacking and the strips are mechanically expanded to form the hexagonal cell honeycomb as shown in Fig. 1a. The initial width and spacing of the bond lines determines the cell diameter (c). Honeycomb made in this fashion has double wall thickness in one direction (L); in other words, it is anisotropic with two principal directions, L and W. Papka and Kyriakides (1998) discuss other effects of the process such as changes to the mechanical properties of the foil material, introduction of residual stresses, small rounding of the expanded corners of the hexagonal cells, and geometric imperfections introduced by small deviations in the bond line spacing and under or over expansion.

The study starts with the presentation of results from compression and crushing experiments on finite size sandwich panels, followed by results from an analytical study of all aspects of the response.

2. Experimental

A series of crushing experiments were performed on Hexcel Al-5052-H39 honeycomb with nominal cell size (c) of 0.375 in (9.53 mm), wall thickness (t) of 0.00374 in (95 μm) and height (h) of 0.625 in (15.9 mm) (Table 1). A consistent deviation from

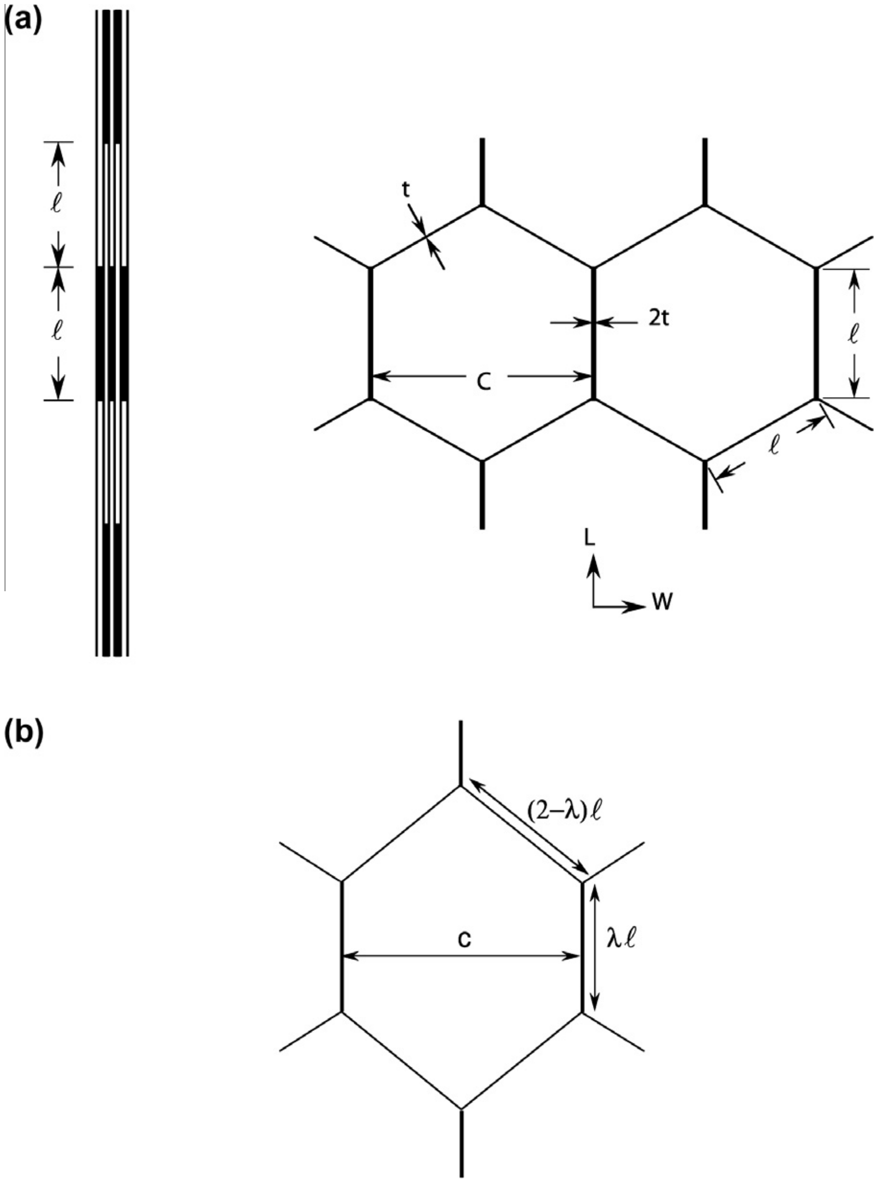

Fig. 1. (a) Laminate of periodically bonded aluminum foils and hexagonal honeycomb microstructure produced by expanding laminate strips. (b) Imperfect hexagonal honeycomb geometry.

Table 1
Geometric parameters of Al-5052-H39 honeycomb used in the experiments.

c in (mm)	ℓ in (mm)	t in (μm)	λ	h in (mm)	L_L in (mm)	L_W in (mm)	τ in (mm)	ρ^*/ρ
0.375 (9.53)	0.2165 (5.50)	0.00374 (95)	0.92	0.625 (15.9)	5.5 (140)	3.2 (81)	0.030 (0.76)	0.026

perfect hexagon arising from a somewhat deficient bond width ($\lambda\ell$ in Fig. 1b) was recorded from measurements of the cell wall lengths. The value of λ quoted in Table 1 is the average from measurements on 30 cells. The relative density of hexagonal honeycomb with double walls in one direction is given by:

$$\frac{\rho^*}{\rho} = \frac{8}{3}\left(\frac{t}{c}\right) \tag{1}$$

(Papka and Kyriakides, 1994). Thus, for the present honeycomb $\rho^*/\rho = 0.026$.

Honeycomb sections typically 8 × 15 cells ($W \times L$) extracted from 24 × 24 in (600 × 600 mm) sheets were bonded to Al-2024-T3 face sheets 0.030 in (0.76 mm) thick (τ) to form sandwich panels approximately 3.2 × 5.5 in (81 × 140 mm) as shown in Fig. 2. A high-strength film epoxy (Hysol EA-9696, 0.060 psf NW) was used, which was cured between platens heated to 250 °F (121 °C) for 90 min.

The panels were compressed in a screw-type testing machine between parallel platens with a ground finish at a displacement rate of $\dot{\delta} = 5 \times 10^{-4} h\,\mathrm{s}^{-1}$. The prescribed displacement and induced load were recorded in a computer based data acquisition system while simultaneously the deformations of the cell walls on two of the sides of the panel were monitored with a video camera.

Fig. 3 shows the stress-shortening response ($\sigma - \delta$) recorded in a typical crushing experiment (dashed line). The nominal stress σ is the force recorded divided by the projected area of the honeycomb ($L_L \times L_W$ in Fig. 2). The initial response is stiff and nearly linear. Along the way, the sides of the hexagonal cells were observed to buckle developing a number of axial waves. The buckling was elastic as the waves would disappear if the panel was unloaded early enough. At higher stress levels inelastic action takes place, a limit load develops, and simultaneously the axial waves tend to localize. The maximum stress achieved was 529 psi (3.65 MPa) which represents the compressive strength, σ_{CO}, of the panel and the onset of crushing. As compression continues the load is seen to drop precipitously down to a local minimum that is associated with the formation of the first local fold. Subsequently, a number of stress undulations develop, which represent the formation of additional folds of the cell walls. The amplitude of the undulations is seen to decrease with δ while the average crushing stress ($\bar{\sigma}_{ch}$) is at a level of 254 psi (1.75 MPa). The particular test was terminated when the panel was crushed down to 40% of its original height and unloaded.

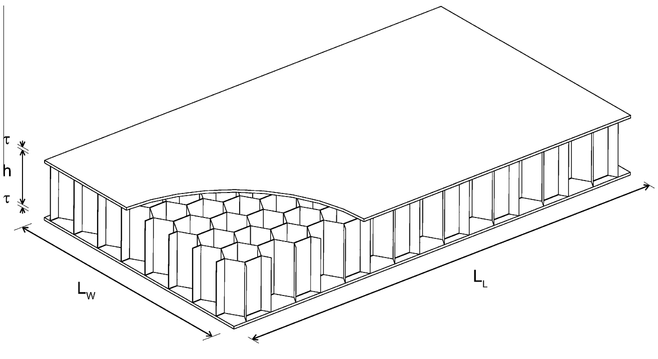

Fig. 2. Three-dimensional rendering of an 8 × 15 cell honeycomb panel.

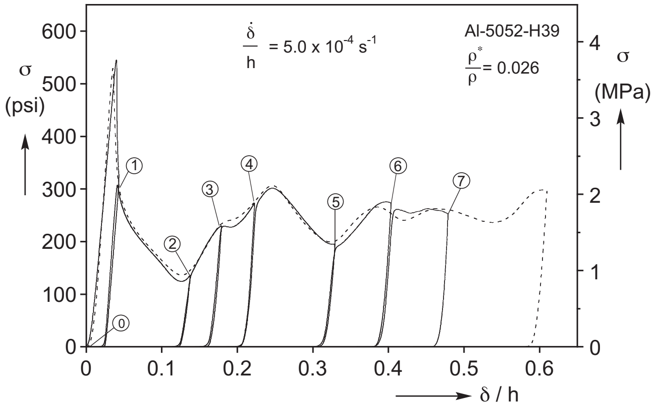

Fig. 3. Axial stress-shortening response for monotonic (dashed line) and step-by-step (solid line) crushing of honeycomb panels.

Several similar tests were performed and the results were found to be quite repeatable. A separate experiment was conducted in order to document the details of the crushing behavior of cell walls. A larger panel 6.5 × 6.2 in (165 × 157 mm) was used for this purpose (Floccari, 2008). The $\sigma - \delta$ response recorded is drawn in Fig. 3 with a solid line. The crushing was performed in a step-by-step fashion so that the specimen was unloaded after a certain amount of deformation. A small section of it (about 5 × 5 cells) was then removed from the panel by cutting along the L and W directions with a diamond saw, keeping the remainder for further crushing. The two cut faces of the removed sections were polished and photographed using a low magnification microscope. Thus for example, the first unloading was performed when the stress dropped to about 300 psi (2 MPa) following the onset of collapse (point ① on the response in Fig. 3). The corresponding pair of photographs taken of the orthogonal faces is depicted as ① in Fig. 4. From left to right the images correspond to the W and L planes of the honeycomb. The deformation is seen to have localized into a single wave symmetrically deployed about the mid-height. On the left, the single walls are bending alternately in and out of the page while on the right the double walls are bending inwards. It is interesting to observe that in the W plane image the double walls have debonded over a length of 0.1h at mid-span (noted also in Wierzbicki (1983) and others).

The specimen was then reloaded, crushed to point ② just after the first load trough, unloaded again, and a second small section was removed in a similar fashion. The two internal planes were photographed and the corresponding images are depicted as ② in Fig. 4. The mid-span deformation has now evolved into folds with some contact developing between the fold walls (see L image). This contact is responsible for the upswing in the overall load. The debonding observed in the W image in ① has been arrested and is seen to be limited to the crease of the fold.

In the next loading step, the stress continues to increase until point ③ when the stiffness of the honeycomb develops a point of inflection. This event is short-lived and the stress quickly begins

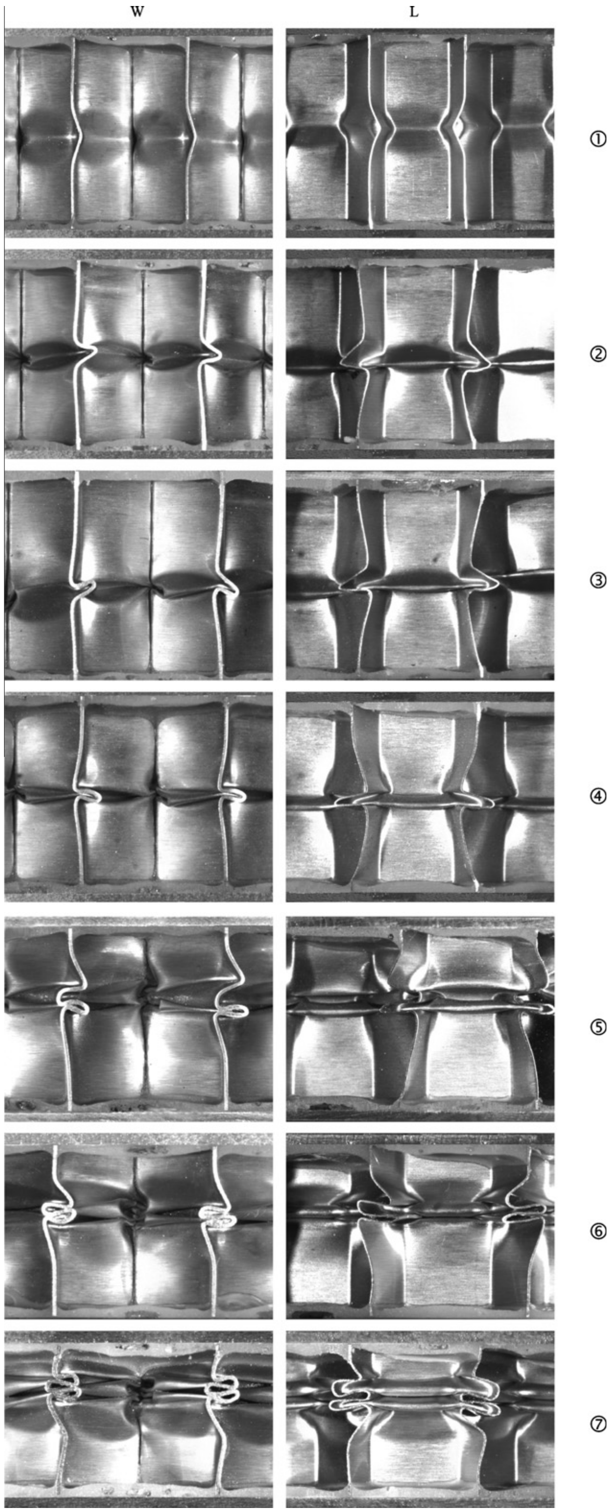

Fig. 4. Sequence of photographs of honeycomb cells at different stages of crushing corresponding to numbered points on response in Fig. 3 (views of *W* and *L* planes).

to rise again, reaching point ④ at $\delta/h \approx 0.22$. As pointed out above, in the neighborhood of ② initial contact occurred on the bottom side of the folds in *L*. As crushing progresses, that side of the fold comes into full contact so that at ③, there is no longer any gap underneath the fold. Subsequently, the other half of each cell collapses until by ④ contact is achieved on both sides. Between these points, the stiffness dropped slightly because crushing occurred where the microstructure was not in self-contact. With the fold in full contact the load increases once more.

With further crushing the load reaches a second peak that is associated with the initiation of a second fold at the top half of the cells, thus breaking the symmetry of the deformation. The load drops tracing another valley at the bottom of which the specimen is unloaded once more and a new small section is removed. The formation of the second fold is clearly seen in images ⑤. (Events reminiscent of those observed in progressive crushing of single tubes—e.g. see Wierzbicki et al. (1992), Bardi et al. (2003))

As the panel is crushed further the load goes through a third peak and is unloaded at ⑥. The beginning of the formation of a third fold in the upper half can be seen in images ⑥. By point ⑦, the third fold is fully developed and a new one starts in the bottom half that hitherto stayed essentially intact. The formation of the new fold is again associated with a stress peak but, as evidenced in Fig. 3, the amplitude of the stress undulations is decreasing as crushing progresses further.

It is worth noting that the progressive removal of a small section of the panel to facilitate observation of the evolution of crushing was undertaken in order to analyze crushing in the interior of the specimen. It was thought that free edges might crush somewhat differently. After each section was removed the area of the specimen was adjusted and this was accounted for in evaluating σ.

It is interesting to observe that the incremental response in Fig. 3 is in very good agreement with the one corresponding to monotonic crushing despite the difference in the size of the two panels. This agreement was generally repeated for most of the panels tested despite some variation in the folding patterns that developed in each. That is, in some specimens the folding developed in the upper half of the honeycomb height first and in others in the bottom. In some cases, part of the specimen crushed in the former manner, part in the latter, and the two zones were joined by a transition with inclined folds. No significant effect from the size of the panel was noticed at least in the range of sizes considered (8 × 15 to 15 × 15 cells).

A total of 8 such experiments were conducted and the differences between them were relatively small. In Table 2 we report the mean values of the collapse stress and of the average crushing stress. The average collapse stress is 539 psi (3.72 MPa) with one standard deviation being 38.1 psi (263 kPa). Since among other factors the onset of collapse is influenced by small initial geometric imperfections specific to each test, the variation is considered to be rather small. The average crushing stress $\bar{\sigma}_{ch}$ is defined as the mean value of the stress level measured starting from δ/h corresponding to the inflection point in the response following the first load depression to δ/h of 60% as shown in Fig. 5. The average of the crushing stresses and one standard deviation from 8 experiments are reported in Table 2.

The mechanical properties of the honeycomb Al-5052-H39 foil were measured using tensile tests on small dogbone specimens extracted from the single wall sides of the hexagonal cells. The elastic modulus was found to be very close to 10^4 ksi (69 GPa) and the yield stress 36 ksi (248 MPa). Because of their relatively small wall thickness (95 μm), soon after yielding the specimens developed shear bands and failed at average strains of about 5% (see Section 2.1.3 in Floccari, 2008).

Table 2
Average values of collapse and crushing stresses from experiments performed.

	σ_{CO} psi (MPa)	$\bar{\sigma}_{ch}$ psi (MPa)
Average	539 (3.72)	241 (1.66)
Standard deviation	38.1 (0.263)	8.3 (0.0572)

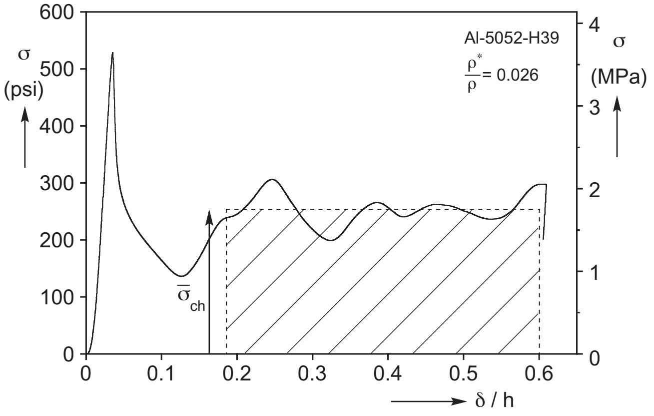

Fig. 5. Definition of the average crushing stress, $\bar{\sigma}_{ch}$.

3. Analysis

The complex compressive response and crushing of honeycombs observed in the experiments is simulated using representative finite element models. The problem complexity is reduced by neglecting the mechanical property changes and residual stresses, left behind by the mechanical expansion process through which the honeycomb is manufactured. Furthermore, the small rounding of the corners of the actual cells is also neglected (these issues are addressed separately in Jang and Kyriakides (2010)). Thus, we will consider the idealized geometry shown in Fig. 6a that consists of perfect hexagonal cells of diameter $c\left(=\sqrt{3}\ell\right)$ and foil thickness t. The double wall thickness of the sides in the L direction is retained but the bonding of the two walls is neglected making them instead monolithic of thickness $2t$. Because of the periodicity of the idealized microstructure, many of the mechanical characteristics of interest can be simulated using a representative unit cell assigned appropriate periodicity conditions. The unit cell chosen is drawn with a dashed line in the L–W plane in Fig. 6a and is depicted in a three-dimensional rendering in Fig. 6b. It has a cross sectional area of $\sqrt{3}\ell \times 3\ell/2$. (The "Y" representing one half of this domain and even one half of the Y can also serve as periodic unit cells. Our choice is made in order to provide more degrees of freedom during crushing).

The main elastic properties can be easily evaluated from simple considerations. Thus, the elastic modulus E_3^* is given by

$$\frac{E_3^*}{E} = \frac{8t}{3c} = \frac{\rho^*}{\rho}, \tag{2}$$

where E is the modulus of the base material. The two Poisson's ratios are equal to that of the base material ν (Zhang and Ashby, 1992)

$$\nu_{31}^* = \nu_{32}^* = \nu. \tag{3}$$

The shear moduli were first evaluated by Kelsey et al. (1958) using energy methods and shear flow analysis that neglect bending of the cell walls. They are given by

$$\frac{3}{2\sqrt{3}}\frac{t}{\ell} \leqslant \frac{G_{13}^*}{G} \leqslant \frac{5}{3\sqrt{3}}\frac{t}{\ell} \quad \text{or} \quad \frac{9}{16}\frac{\rho^*}{\rho} \leqslant \frac{G_{13}^*}{G} \leqslant \frac{5}{8}\frac{\rho^*}{\rho} \tag{4a}$$

$$\text{and} \quad \frac{G_{23}^*}{G} = \frac{1}{\sqrt{3}}\frac{t}{\ell} = \frac{3}{8}\frac{\rho^*}{\rho}. \tag{4b}$$

The performance of these expressions was evaluated using FE models and the honeycomb parameters listed in Table 1 (perfect hexagonal cell). In the models the honeycomb upper and lower surfaces were restrained to remain plane. The two expressions were found to yield shear moduli that were in very good agreement with those from the numerical results. In the case of G_{13}^* the upper bound was found to be closer to the numerical result than the lower bound (see also Grediac, 1993).

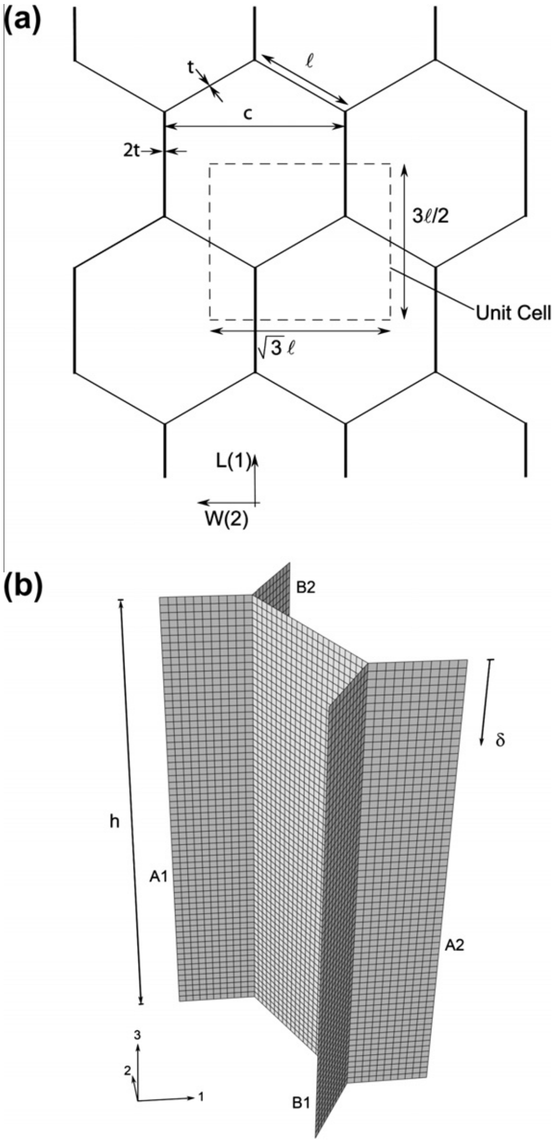

Fig. 6. (a) Honeycomb unit cell used in the calculations and (b) three-dimensional rendering of the cell.

3.1. Finite element models

We will start by considering just one fully periodic unit cell; limiting effects of this choice of domain will be discussed subsequently. The unit cell is discretized within the nonlinear FE code ABAQUS using S4 shell elements. S4 is a fully integrated 4-node element that allows for finite membrane strains. Progressive folding that characterizes the crushing calculations is numerically intensive so the shell element selection and the discretization adopted were guided by computational efficiency. A regular mesh with nearly square elements was adopted, while the number of elements used was selected from convergence studies that follow.

For the panels tested a thin film of epoxy is used to bond the faceplates to the honeycomb. When cured the epoxy tends to form meniscus-like fillets at the corners between the cell walls and the plate. After looking into the effect of the fillets on the calculated response it was decided that including them would make the calculation numerically cumbersome without adding significantly to the accuracy of the predictions. Thus, the top and bottom edges of the unit cell are assumed to be fixed, except that the top can translate in the x_3-direction.

The following periodicity conditions are used for the four lateral edges of the unit cell. Define the edges as (A_1,A_2) and (B_1,B_2) as shown in Fig. 6b. The displacements and rotations of points on these edges are respectively denoted by (u_{i1}, u_{i2}) and $(\theta_{i1}, \theta_{i2})$ $i = 1$, 3. The following relationships are prescribed for the degrees of freedom of points on each pair of faces:

$$u_{i1} - u_{i2} = u_{i1}^{ref} - u_{i2}^{ref} \quad \text{and} \quad \theta_{i1} - \theta_{i2} = 0, \quad i = 1, 3, \tag{5}$$

where u_{ij}^{ref} are displacements of conjugate points on opposite sides chosen as reference points. Eqs. (5) hold for every node on the four lateral edges, with the exception of the 8 nodes that are also contained in the top and bottom edges, which are required to satisfy the prescribed boundary conditions.

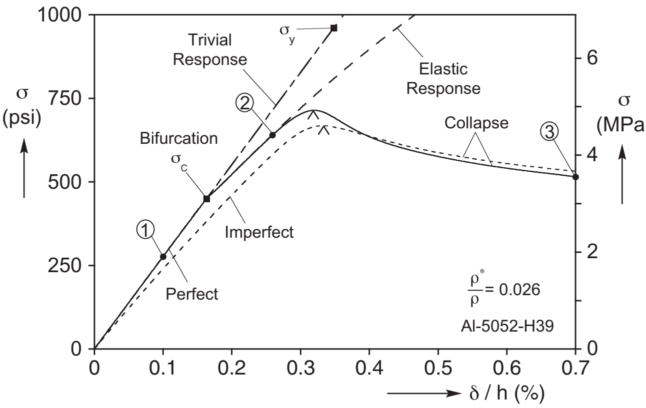

Fig. 7. Initial stress-shortening responses for perfect and imperfect characteristic cells.

The material is modeled as a finitely deforming J_2 solid that hardens isotropically. The model is calibrated to a bilinear stress–strain response that was fitted to measured tensile tests on the honeycomb foil. It has an elastic modulus of 10^4 ksi (69 GPa), a yield stress of 36 ksi (248 MPa), a post-yield modulus of 57 ksi (394 MPa) up to a strain of 10% and is perfectly plastic at higher values (true stress-logarithmic plastic strain version).

3.2. Buckling and initial postbuckling behavior

The cell is loaded by prescribing incrementally the normal displacement of the top surface δ. A typical calculated compressive stress-displacement ($\sigma - \delta/h$) response is shown in Fig. 7, where σ is the force divided by the cell's projected area $(3\sqrt{3}\ell^2/2$, see Fig. 6a; calculations of this type are performed in ABAQUS standard with a mesh of 18254 elements). The response is initially stiff and linear with stiffness E_3^* as quoted in (2). At some level of stress (σ_C = 428 psi—2.95 MPa) the plate-like walls of the cell buckle into the mode shown in Fig. 8a. It has three half waves along the height of the cell and is symmetric about the mid-height. Interestingly, the second buckling mode shown in Fig. 8b is anti-symmetric about the mid-height and occurs at the only slightly higher stress of 434 psi (2.99 MPa). It is worth noting that higher modes are separated by larger stress levels. Buckling is clearly elastic as the honeycomb yields at a much higher stress level marked on the extended trivial response with a square symbol (σ_y = 947 psi—6.60 MPa). The critical buckling stress of 428 psi (2.95 MPa) compares with the upper bound value developed by Zhang and Ashby (1992) of 1249 psi (8.61 MPa) (see also §4.5 Gibson and Ashby, 1997). The bound was developed using a long strip of foil width ℓ and thickness t with fixed boundary conditions along the long edges. It is interesting to note that even if the sides had been

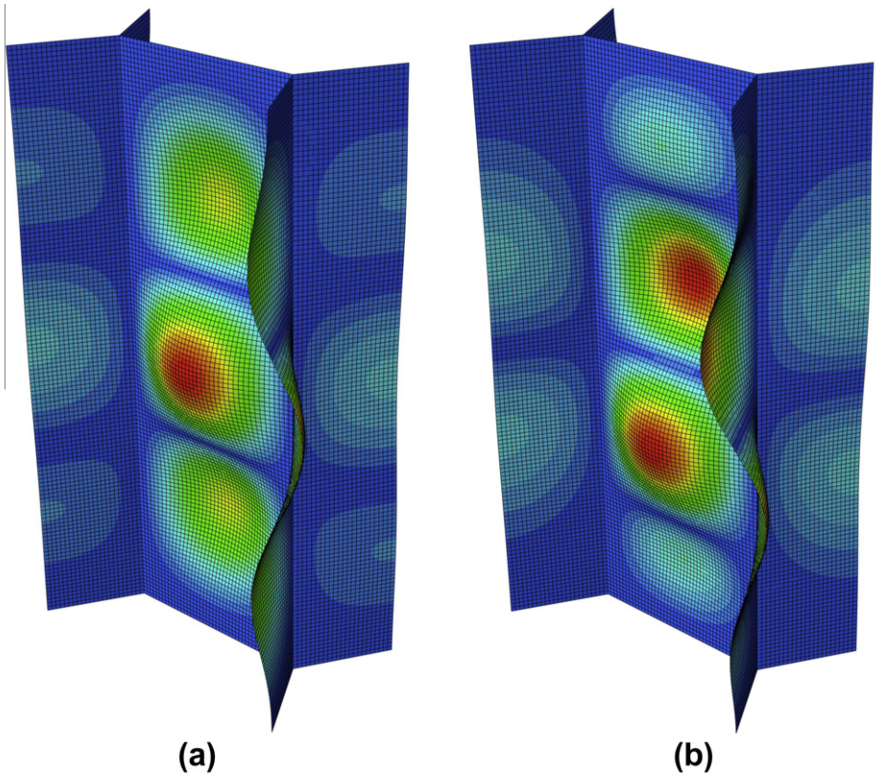

Fig. 8. First (a) and second (b) buckling modes.

assumed to be simply–supported, the buckling stress from this approach would still be significantly higher than the numerical value (717 psi—4.85 MPa; using $K = 3.29$ in Ref. Eq. (7)). Since the cell corners are not rigid, neighboring cells buckle in a compatible manner (see Fig. 8), which apparently makes the structure more flexible.

Elastic buckling of plates has a stable postbuckling response and consequently the initial change in stiffness of the buckled structure is relatively small. Fig. 9 shows deformed configurations corresponding to three points on the response marked with numbered bullets in Fig. 7. Configuration ① is in the pre-bucking regime and so the honeycomb does not exhibit out of plane deformations. In configuration ② the symmetric deformation of mode 1 is clearly discernible. The postbuckling response is of course nonlinear but the structure remains elastic until a higher stress level is reached. With further compression, the combination of bending and membrane stresses yields the material and the response starts to lose stiffness deviating from the elastic one (drawn with dashed line). Plastification eventually results in the development of a load maximum in the response that represents the collapse load of the structure ($\sigma_{CO} = 714$ psi—4.93 MPa). This value of collapse stress is somewhat higher than the average value measured in the experiments of 539 psi (3.72 MPa). Various imperfections present in real structures tend to reduce the collapse load (see imperfection sensitivity studies in Section 4). The effects of the size of the domain analyzed and of the mesh will be discussed in Section 4.

With further compression the deformation starts to localize while the average stress follows a downward trajectory. In configuration ③ in Fig. 9 the deformation is seen to localize, but remains symmetric about the mid-height (compare amplitude of displacements at mid-height and elsewhere). The continuation of the collapse of the structure and the subsequent progressive folding of the walls will be discussed in the next section.

At this stage it is also interesting to consider the response of an imperfect version of this unit cell. The imperfection chosen here corresponds to the first buckling mode (see Fig. 8a) with the point of maximum transverse deflection assigned an amplitude equal to t. The response of the imperfect structure, drawn in Fig. 7 with a dashed line, is seen to be initially somewhat less stiff than the one for the perfect geometry. The load maximum is 6.5% lower but at higher deformations it merges with the perfect case response.

In reviewing the literature we observed that the distinction between "buckling" and "collapse" is rather blurred. This is partly due to the fact that the onset of buckling in the cell walls is difficult to pinpoint experimentally. Measured responses appear more like the one for the imperfect cell model in Fig. 7 in which the point of buckling is impossible to identify. The best one can do is to bracket σ_C by careful monitoring the development of waves in the cell walls, something that is practically difficult to perform and consequently not usually done. Instead, some quote the maximum stress recorded as "buckling." As reported above, the load maximum is caused by inelastic action due to the combined effect of cell bending and compression. In the present case the nonlinearity is loss of stiffness due to plasticity; in others it could be some type of damage that can lead to failure. In both cases a non-trivial calculation is required to pinpoint the load maximum. A reasonable lower bound of the collapse load may be established by calculating the onset of yielding due to combined bending and compression in the fashion proposed by Timoshenko. Finally, we note that as c/t decreases, buckling can occur in the plastic range of the material requiring a different treatment from the present one.

3.3. Crushing response

Honeycomb crushing involves severe local bending of and contact between the walls of the folds. Consequently, in contrast to the prebuckling and initial postbuckling calculations described in Section 3.2, crushing was performed using ABAQUS/Explicit due to the computational efficiency that it affords. The basic calculations involve the characteristic cell shown in Fig. 6b with a mesh of 5850 S4 elements (convergence study will follow in Section 4). The cell is assigned the periodicity conditions given in (5). The top and bottom edges are fixed except in the x_3-direction of the top edge, which is prescribed a downward displacement. This displacement was assigned a "smooth step" time function in order to minimize inertial effects, thus mimicking the "quasi-static" rate of crushing of the experiments. Furthermore, the computation

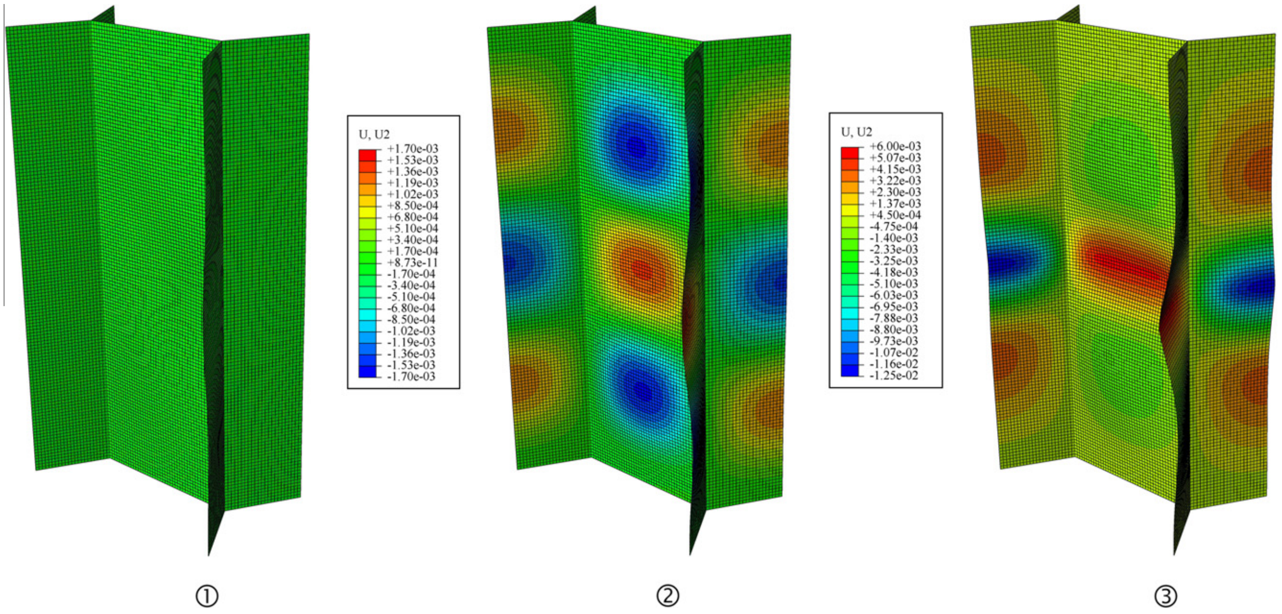

Fig. 9. Deformed configurations corresponding to numbered bullets on the perfect geometry response in Fig. 7.

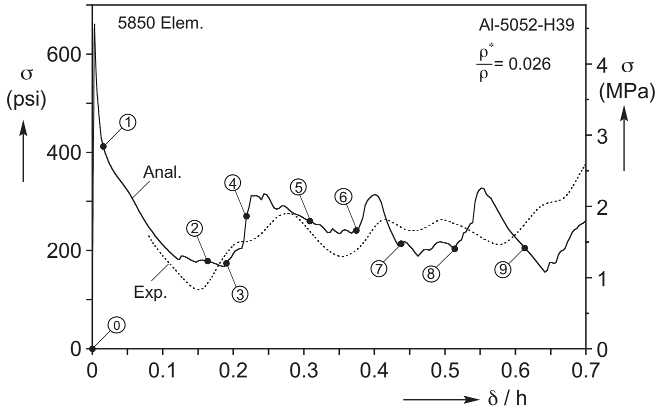

Fig. 10. Comparison of a crushing response from unit cell calculation and experimental one.

time was minimized by speeding up the simulation to a total crushing time of 2 s. For this choice of crushing time, the kinetic energy of the structure was shown to remain only a small fraction of the strain energy, thus confirming that the simulation remained quasi-static. The same time independent constitutive model described in Section 3.2 was adopted for the mechanical properties of the Al-5052-H39 alloy.

The crushing involves contact between folds of adjacent cell walls as well as self-contact and consequently both sides of the cell walls were considered for contact (ABAQUS' "all exterior" parameter). This process ensures that contact occurs at the actual surface of the walls (i.e., at ±$t/2$). Suffices to say that for such problems contact constitutes a major contributor to the total computation time of the simulation.

A typical crushing response from such a simulation is shown in Fig. 10 along with one of the experimental responses. Fig. 11 shows W and L pairs of views of the initial and a set of deformed

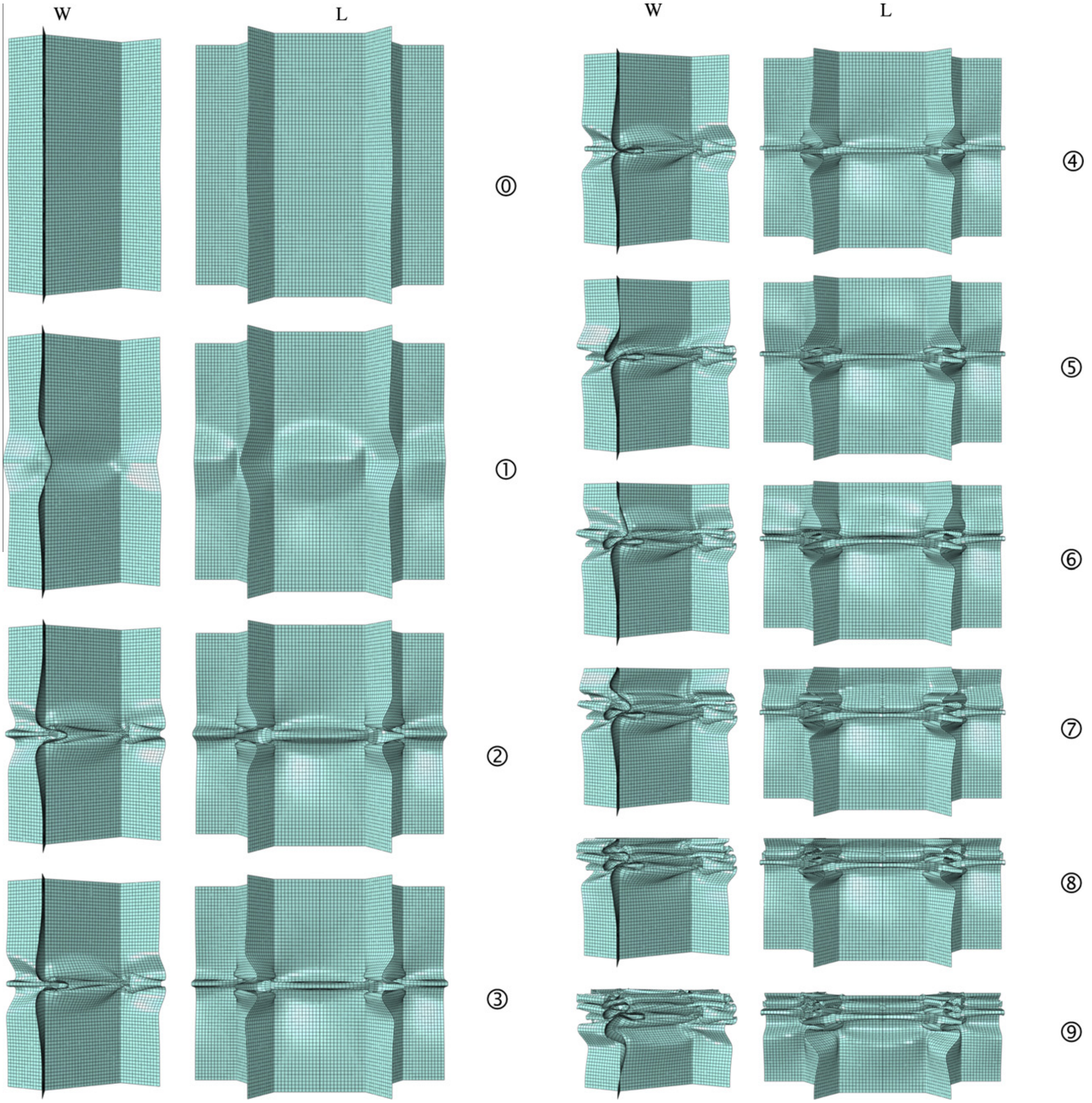

Fig. 11. Deformed configurations of the unit cell at different degrees of crushing corresponding to numbered bullets on the calculated response in Fig. 10 (views of W and L planes; L views have been doubled for better visualization).

configurations of the unit cell corresponding to the numbered bullets marked on the response in Fig. 10. An initial imperfection corresponding to the first buckling mode (Fig. 8a) with amplitude of *t* was included in the model to ensure consistency in the initial mode of collapse with the results shown above. Configurations ①, on the first descending part of the response, show localized deformation symmetrically deployed about the mid-height that is associated with the initial stages of collapse of the cell. The local buckles that have formed are inward in the *W* side and outward in the *L* side. Simultaneously, the walls above and below the collapse are seen to be relatively undeformed. In the experiments the first sign of some debonding of double walls was observed at this stage. Wall separation was precluded in this model and this omission is expected to introduce some minor differences between the calculated and measured responses.

The collapse continues with folding up the local buckles at mid-height while the load is decreasing. In the neighborhood of configuration ②, contact between folds in adjacent walls develops for the first time. The structure is stabilized and this is reflected in the bottoming out of the response. In the neighborhood of configuration ③, self-contact in the folds takes place further stabilizing the structure and the load takes an upward trajectory (note that the images show the mid-surface of the cell). It is reassuring that the depth of the load trough is similar (slightly higher) to that of the experiment.

The inflection point that was consistently seen in the experiments is reproduced in the simulation but is less distinctive. We speculate that in the physical test it may be a manifestation of the contact of the separated parts of the double walls that can be seen in configuration ④ in Fig. 4. In configuration ④ some of the folds have developed self-contact and the upward trend in the load continues. At some point the thus far intact part of the upper half of the cell gets destabilized once more; a new load maximum develops and a second fold is initiated from the disturbance provided by the bent walls of the first one. The new fold can be seen at a well-developed state in ⑤. The second load peak is at a slightly higher level than the experimental one. By configuration ⑥, contact is fully developed in the second fold and the response takes an upward path once more. A third load peak develops at about the same level as the second one. This is associated with the initiation of a third fold again in the upper half of the cell that can be seen in configuration ⑦. Contact arrests the deformation in the third fold and the response recovers once more. Configuration ⑧ shows the third fold fully developed and the stiffening of the corresponding response once more. A fourth load peak develops which signals the commencement of folding in the lower half of the cell which can be seen in configuration ⑨ just before the next load valley. The folding in the lower half continues forming a total of five folds before densification, which agrees with the experiment. However, the experimental response associated with the final folding differs from the simulation primarily because of the presence of the epoxy fillets that form at the interfaces with the plates.

Overall, the simulated crushing response is a reasonable reproduction of the experimental one all be it with some differences. The crushing stress ($\bar{\sigma}_{ch}$ = average σ between $0.225 \leqslant \delta/h \leqslant 0.60$) is 257 psi (1.77 MPa), that is 8.4% higher than the mean value from the experiments. The period of the folds is somewhat different than the experimental one and the decay in the amplitude of the stress undulations was not captured here as stress peaks 2, 3 and 4 occur at about the same level. Furthermore, small amplitude undulations associated with local events within the folds appear in the calculated response making it more rugged. Of course, the experimental response represents the average over many cells (at least 8×15), which tends to smooth out local force fluctuations.

4. Parametric study

We consider again separately the two major aspects of honeycomb compressive behavior buckling and collapse, and crushing and try to establish their sensitivity to various problem parameters. The parameters considered include mesh sensitivity, the size of the domain analyzed, and several types of geometric and other imperfections.

4.1. Effect of mesh and domain size on buckling and collapse

The effects of the mesh density used in the characteristic cell on the bifurcation and collapse stresses was examined and the results are shown in Fig. 12, where the two variables are plotted against the number of S4 elements, *M*, used. In all cases the mesh is nearly square. The calculated critical loads are normalized by the bifurcation buckling stress, "σ_C", for what we designate as the "basic" mesh of 4224 elements which is 437 psi (3.02 MPa; normalized value designated as $\bar{\sigma}_C$). The coarsest mesh considered has 870 elements, the second 2208, the third 4224 and so on. The buckling stress is seen to gradually decrease with *M* so that for 870 elements it is 4.5% higher than σ_C and for 18254 elements it is 2% lower; this last case can be considered as converged. In other words, the basic case is not fully converged as far as this variable is concerned; instead it has been chosen for computational expediency in the execution of very large calculations that follow. It is important to note however that the mode associated with the critical stress remained the same for all meshes.

Unless otherwise stated, all collapse stress calculations were performed with an initial imperfection corresponding to the critical buckling mode with an amplitude of *t*. The calculated $\bar{\sigma}_{CO}(=\sigma_{CO}/\sigma_C)$ values are seen in Fig. 12 to be less sensitive to the mesh so that even for the coarsest mesh $\bar{\sigma}_{CO}$ is only 0.6% higher than the base case, and for $M > 4224$ the results can be considered to have converged.

As is well known, in periodic structures both the mode and the critical buckling stress can be influenced by the size of the periodic domain considered; or in other words, criticality can involve more than one characteristic cell. Geymonat et al. (1993) developed a method based on Bloch wave theory that automates the search for the critical state (see application to a Kelvin foam in Gong et al., 2005). The method uses the stiffness matrix of the characteristic cell, which for the present problem is large (51000^2 for the unit cell) making the automation afforded by the method difficult to exploit. For this reason here we opt for a more limited examination of the effect of the domain size that involves direct analysis of periodic domains of different sizes.

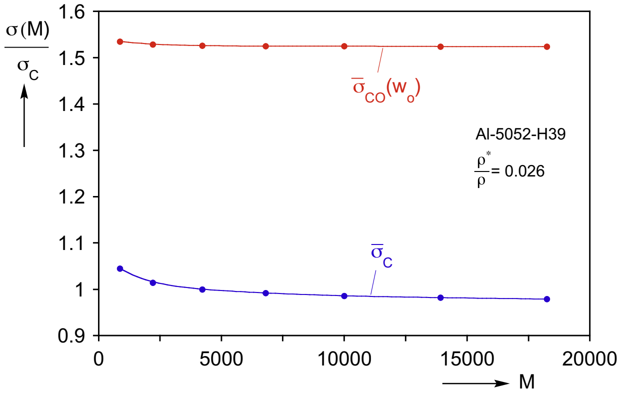

Fig. 12. Calculated buckling and collapse stresses vs. the number of elements used in the unit cell.

In the way of evaluating the effect of the domain size we calculated the critical buckling and collapse stresses of periodic rows of N cells in the W and L directions. Results for rows of 1 to 8 cells are plotted in Fig. 13. In the L direction the buckling stress drops slightly as N increases but appears converged after $N = 5$ at a value that is about 4.5% lower than that of the base case. In the W direction the effect of N on the buckling stress is larger so that it is reduced by about 10% for $N \geqslant 6$. Fig. 14a and Fig. 14b show renderings of the buckling modes for N_L and N_W of 4. The shapes of the modes are the same as for the single cell but the amplitude of the waves is more pronounced in the central cells. Similar variation in amplitude was also observed for longer domains. Included in Fig. 13 are the normalized collapse stresses for W and L rows of periodic cells. Interestingly, this value increases slightly (less than 4%) with N but is essentially constant for $N \geqslant 4$. It is worth noting that the collapse stress of the corresponding perfect domains remained essentially unchanged with the values of N_L and N_W.

In the same spirit we considered periodic square domains with $N_L \times N_W$ (=n) cells. The buckling and collapse stresses are plotted against n in Fig. 15 for $1 \leqslant n \leqslant 64$ (solid lines). Here the number of cells in the periodic domain impacts the buckling stress more significantly; thus, for $n = 36$ the buckling stress is reduced by nearly 19% and remains essentially unchanged for larger n. The critical buckling mode for $n = 16$ is shown in Fig. 14c. Once more the mode imparts the same shape to each cell but the amplitude is more intense in the central cells. This pattern was observed in

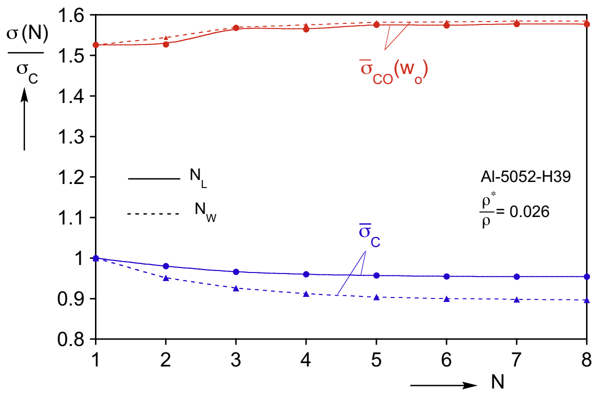

Fig. 13. Calculated buckling and collapse stresses vs. number of cells in periodic rows along L and W directions.

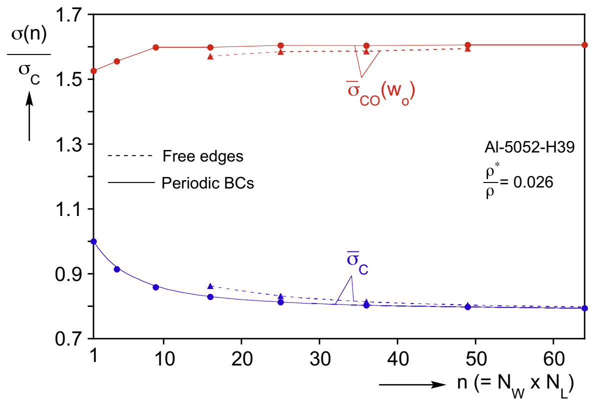

Fig. 15. Calculated buckling and collapse stresses vs. size of square domains with and without periodicity conditions.

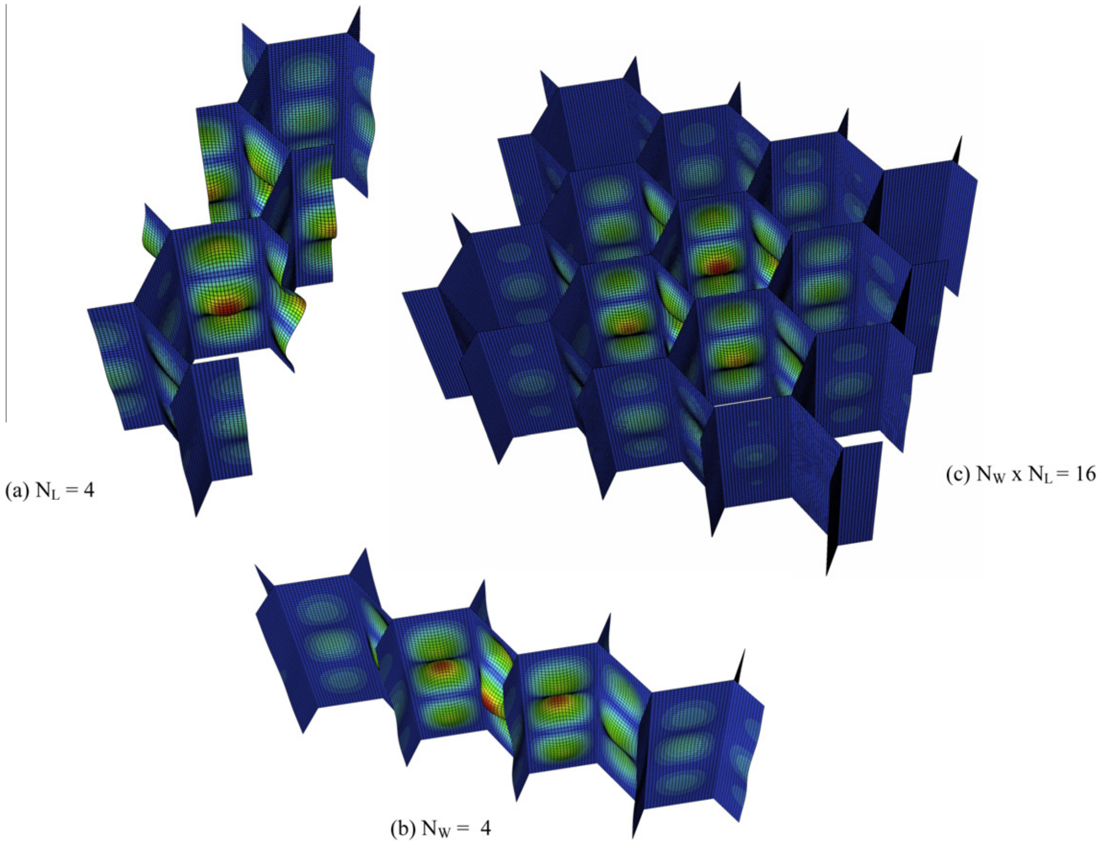
(a) $N_L = 4$

(c) $N_W \times N_L = 16$

(b) $N_W = 4$

Fig. 14. First buckling modes for domains with (a) 4 cells along L, (b) 4 cells along W, and (c) 4×4 cells.

the larger domains considered also. The collapse stress for $w_o = t$ is seen to be insensitive to n for all but the smallest domains.

For domains larger than $n = 16$ calculations were also performed by removing the periodicity conditions from the edges, in other words we considered finite size square domains. The first observation is that the buckling mode consisted of three half waves as in the periodic domains. The corresponding buckling stresses are included in Fig. 15 with a dashed line and are seen to be very comparable to the results from the periodic domains. As expected, the two sets of results converge as n becomes larger. The collapse stresses were also calculated for these cases using again an imperfection with amplitude t. The results are included in Fig. 15 and are seen to be slightly lower than those from the periodic domains.

4.2. Effect of imperfections on collapse

As noted earlier, the collapse stress calculated for a characteristic cell with perfect geometry was higher than the values measured in all of our experiments. It is thus worth examining the effect of various imperfections on this variable (see also Chen et al., 2009). The most natural one is a geometric imperfection in the form of the critical buckling mode shown in Fig. 8a. Fig. 16 shows the collapse stress of the characteristic cell vs. the amplitude of the imperfection w_o normalized by the foil wall thickness (see inset in Fig. 16). An imperfection with amplitude of t reduces σ_{CO} by 7% and for $3t$ by 17%. In other words, the structure is modestly sensitive to this imperfection.

In our experiments the panels were compressed between stiff parallel (nearly) platens. Although care was taken to make the platens as parallel as possible, small misalignments were observed and are thought to have influenced the measured collapse stress. The effect of one directional platen misalignment on the collapse pressure was analyzed using a 4 × 4 periodic cell. The calculated collapse stresses for $w_o = t$ are plotted in Fig. 17 against the single direction misalignment angle ϕ. The results show that even very small misalignments can cause a reduction in σ_{CO}. As might be expected, the direction of the misalignment also influences the collapse stress with larger reduction taking place when ϕ is oriented in the W direction. Thus for example, for $\phi_W = 0.03°$ the collapse stress drops by about 5% and for 0.06° by about 11%.

Papka and Kyriakides (1994, 1998) reported that the shape of expanded honeycomb cells can differ from the perfect hexagonal geometry considered this far. The bond lines that are initially printed on the foil sheets can deviate from the ideal value so that on expansion the hexagonal cells are distorted in the fashion shown in Fig. 1b. In addition, honeycomb can be somewhat under- or over-expanded. These two manufacturing "imperfections" affect the density of the honeycomb as well as all its mechanical properties. Measurements performed on the honeycomb used in this study showed that the value of the cell width c was consistently very close to the ideal value of 0.375 in (9.53 mm). However, some variations in the bond line length were found. For this reason we used unit cell calculations to examine how the bond line length affects the buckling and collapse stresses. Fig. 18 shows plots of calculated buckling and collapse stresses against the bond line deviation parameter λ ($0.8 \leqslant \lambda \leqslant 1.05$ with 1 representing the ideal bond line length). Both critical stresses decrease for $\lambda < 1$ and increase for $\lambda > 1$ with the buckling stress being affected more by this variable than σ_{CO}.

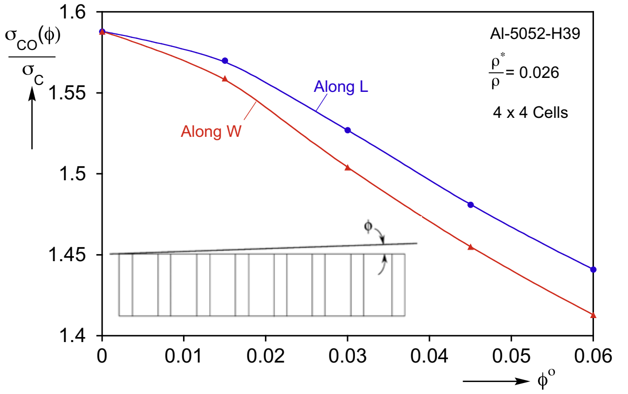

Fig. 17. Calculated collapse stress vs. platen misalignment angle along L and W directions (4 × 4 cell domain).

4.3. Parametric study of crushing

Next we conduct a limited parametric study of the crushing response as a whole as well as the crushing stress as defined in Fig. 5. Figure 19 compares the crushing responses of a single characteristic cell using three different nearly square mesh densities. As reported above, the collapse is not particularly sensitive to the mesh densities considered here (see Table 3). The subsequent crushing response however is seen to be the highest for 2700 elements, lower for the base case mesh of 4224 and slightly lower yet for 5850. Consequently the crushing stresses calculated for each also differ as shown in the table below. The formation of the sharp folds associated with crushing requires a fine enough mesh for it to be accommodated. Indeed, some of the details of the folding tend to differ when the mesh is not sufficiently refined. These numbers compare with an average crushing stress of 241 psi (1.66 MPa) from our experiments.

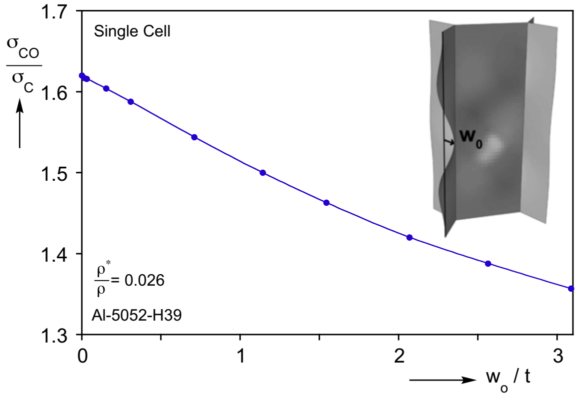

Fig. 16. Calculated collapse stress vs. amplitude of initial imperfection corresponding to the critical buckling mode.

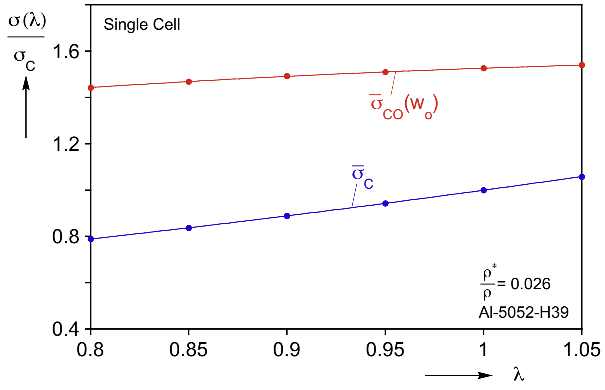

Fig. 18. Calculated collapse and buckling stresses vs. bond length imperfection parameter λ.

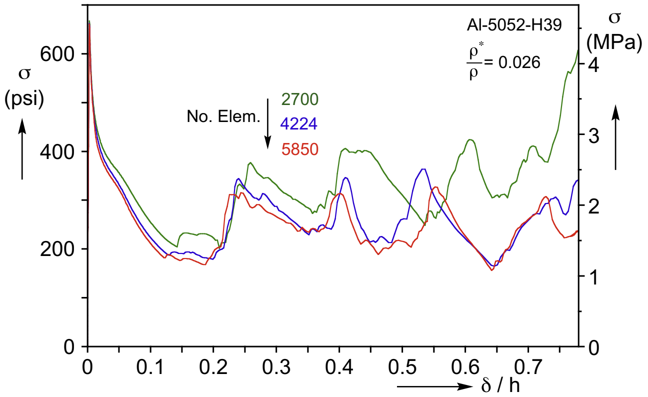

Fig. 19. Calculated axial stress-shortening responses from unit cells with various meshes.

Table 3
Calculated collapse and crushing stresses for different mesh densities.

Element No.	σ_{CO} psi (MPa)	$\bar{\sigma}_{ch}$ psi(MPa)
2700	668 (4.61)	330 (2.28)
4224	667 (4.60)	267 (1.84)
5850	667 (4.60)	257 (1.77)

The effect of the domain size on the crushing response was evaluated using the following periodic domains: $\{N_W \times N_L\} = \{1 \times 1, 1 \times 4, 4 \times 1, 4 \times 4\}$, with each cell in each domain having the same mesh as the base case (4224 elements). The stress-shortening results are plotted in Fig. 20 together with one of the experimental responses. Fig. 21 shows four deformed configurations of the 4 × 4 domain corresponding to the numbered bullets on the response in Fig. 20. Once again, the four collapse stresses differ by a small amount (see Table 4) with the larger domains having somewhat higher values. The initial collapse responses through the first stress trough and up to the second load peak are identical. This is because deformation localizes in the same manner at mid-height for all domains (e.g., compare ① in Figs. 21 and 11a). The formation of the first fold is also similar (e.g., compare ② in Figs. 21 and 11a). Differences between the responses from the three smaller domains and the larger one (4 × 4) start with the formation of the second fold. While for the first three domains the second fold occurs strictly on either the top or the bottom half of the height (see, ⑤ and ⑥ in Fig. 11b), the events for 4 × 4 are different (corresponding configurations from 1 × 4 and 4 × 1 domains are very similar to the results in Fig. 11b and are not included here for brevity). Careful examination of configuration ③ in Fig. 21 shows that the position of the second fold differs from the left to the right. On the left it is developing in the lower half of the cells and on the right in the upper half. The third load peak occurs at the same displacement for all domains but it is distinctly lower for the larger one. Configuration ④ in Fig. 21 shows the crushing at a more developed stage, and at the same time illustrates even more clearly the difference in the crushing patterns across the domain. It is worth noting that the difference in the crushing patterns develop inside the domain as opposite edges must maintain the imposed periodicity conditions. Thus, for the observed difference in folding patterns to develop, several folds are inclined something that is not observed in the smaller domains. Note that such a variation in the position of folding along the height of the specimens was also observed in most of the crushing experiments performed albeit in much larger domains with free edges.

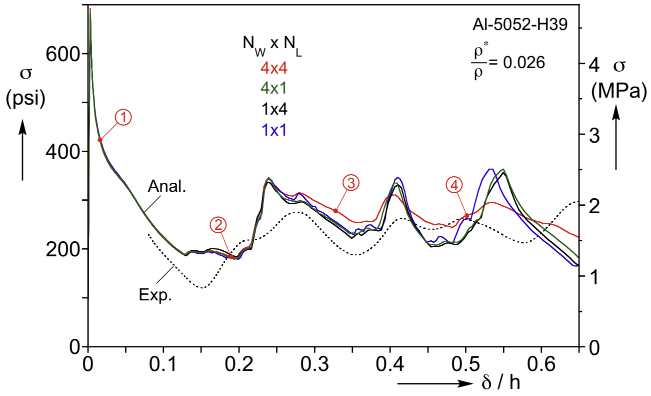

Fig. 20. Calculated axial stress-shortening responses for various domain sizes along with an experimental one.

The response of the larger domain continues to deviate from the others at larger values of δ with the last load peak being even lower than those of the other three domains. Another difference is that the larger domain response is less rugged. The decay in the amplitude of the stress undulations as well as the smoothness of the response of the larger domain are both features that are observed in the experimental responses also (e.g., see case included in Fig. 20). Apparently, these aspects of the response are related to the variation in the crushing patterns within the domain. This variation causes the collapse of cells and the contact between the walls of the folds to occur at somewhat different times across the domain; these have the effect of first smoothening the response and second of causing a decay in the amplitude of the average stress undulations. At the same time however the average stresses of the responses of the four domains considered do not differ as is evident from the crushing stresses reported in Table 4.

The 4 × 4 domain discussed is already rather large and computationally intensive. Larger domains were considered and the trend was similar. Crushing of large domains with free edges was not performed as experimentally the effect of the free edges was found to be modest at least for the sizes considered.

In summary then, the crushing of a single characteristic cell and of small linear domains results in stress undulations of nearly the same amplitude and in more rugged responses. Switching to a square domain of 4 × 4 cells smoothens the response and causes a progressive decay in the stress undulations, both features that were observed in the experiments. However, all domains considered yielded about the same crushing stress, which happens to be somewhat higher than the measured values. One cause of this difference may be the debonding observed to occur at least during the formation of the first fold in the experiments; debonding was not included in the present calculations.

5. Summary and conclusions

The paper presented results from a comprehensive study of the compressive response and crushing of Al-5052-H39 honeycomb panels. The honeycomb used had a cell size of 0.375 in (9.53 mm), a relative density of 0.026, and a height of 0.625 in (15.9 mm). Finite size panels of the order of 8 × 15 cells or larger were compressed quasi-statically between flat platens. Following an initial linear response, the cell walls buckle elastically. The postbuckling response is initially stiff and stable but inelastic action progressively softens it leading to a limit load instability. Deformation localizes first at mid-height in the form of a sharp buckle, which with the load

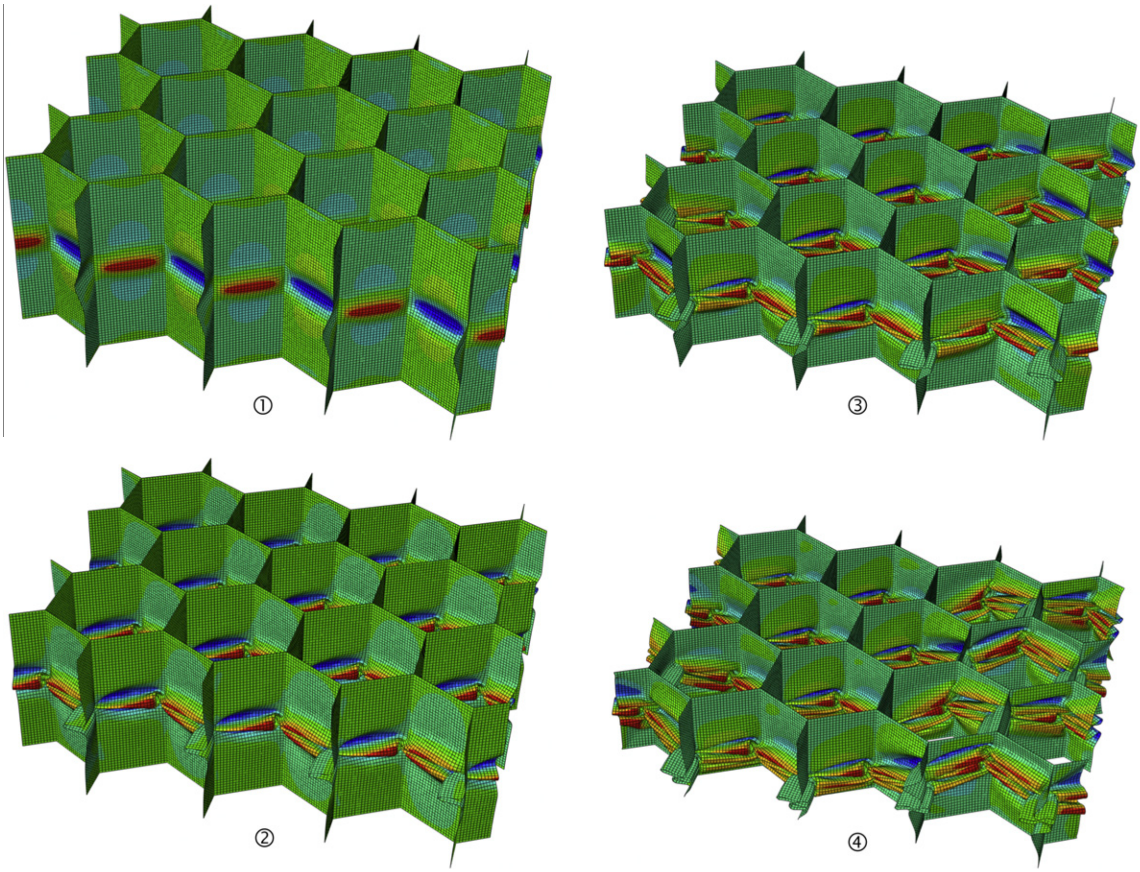

Fig. 21. Deformed configurations corresponding to numbered bullets on the response of the 4 × 4 cell domain in Fig. 20.

Table 4
Calculated collapse and crushing stresses for different periodic domain sizes.

Domain Size $N_W \times N_L$	σ_{CO} psi (MPa)	$\bar{\sigma}_{ch}$ psi(MPa)
1 × 1	667 (4.60)	267 (1.84)
1 × 4	684 (4.72)	265 (1.83)
4 × 1	688 (4.74)	265 (1.83)
4 × 4	699 (4.82)	271 (1.87)

continuing to drop morphs into a fold. When the walls of the fold come into contact local collapse is arrested, the load begins to recover, and a second fold develops on one side of the first one. The second fold in turn collapses forming a new load peak and a second trough. This progressive folding keeps repeating until the whole panel is consumed and the structure returns to a stiff response.

The compressive response including the buckling, collapse and crushing have been simulated numerically using finite element models of various domain sizes. The models idealize the microstructure as hexagonal, with double walls in one direction. Several of the properties of interest can be extracted using a characteristic cell that exploits the periodicity of the microstructure. Closed form expressions for the elastic moduli from the literature were compared to the numerical predictions and found sound. Buckling was confirmed to occur in the elastic regime of the material at stress levels that are much lower than values reported in the literature that are based on simplistic models. The postbuckling response is stable and stiff as is expected from the plate like strips that constitute the walls of the hexagonal cells. Combined membrane and bending stresses eventually yield the material and the response develops a limit load, which represents the compressive strength of the honeycomb. For the particular honeycomb studied, the collapse stress was 67% higher than the buckling stress.

The buckling and collapse stresses were found to be sensitive to some degree to the mesh density used. The collapse stress was shown to be mildly sensitive to geometric imperfections including small misalignment of the compression platens used in the crushing. In view of this sensitivity the predicted collapse stress is considered to be in good agreement with measured values.

Beyond the limit load, deformation localizes first into a single sharp buckle at mid-height as was observed in the experiments. With further compression the buckle evolves into a fold. The downward trajectory of the response stops when the walls of the fold come into contact. The response then returns to positive stiffness and remains so until a second fold starts to develop either above or below the first one precipitating a second load peak followed by a stress valley. The load recovers again when a third fold develops and this repeats until the whole domain is folded up. In the experiments, the amplitude of such stress undulations consistently decayed as the crushing progressed, whereas in the single cell predictions it stayed nearly unchanged. The mean value or crushing stress however was found to be about 8% higher than the average of 8 experimental values. This level of agreement however came only with the use of a fine mesh, which is required in order to capture the details of the sharp folds. Another difference between the single cell predictions and the measurements is the much more rugged nature of the calculated response. The debonding observed in the experiments to occur at least during the formation of the first fold was not modeled. It is not expected to affect the collapse stress but should have some influence on the crushing stress. The expansion process through which honeycomb is manufactured introduces small geometric variations, residual stresses, and changes in mechanical properties. This effect will be addressed separately in a follow up publication.

The size of the periodic domain considered in crushing calculations was found to influence the results as follows. When a 4 × 4 cell periodic domain was crushed, the buckling and initial localization that follows collapse were found to replicate those of the single cell. However, the height location of the subsequent folding varied across the domain, a feature that is commonly observed in experiments. This variation in the location of the folds had the result of first smoothening the crushing response and second of introducing a decay in the amplitude of the stress undulations, both features that mimic the experimental results. The mean value of the stress undulations however, in other words the crushing stress, remained unaffected.

In view of the results presented we conclude that the compressive response of honeycomb from the initial elastic part, through buckling, collapse and crushing can be evaluated with engineering accuracy using one characteristic cell. We point out however that the crushing response requires a fine mesh for it to be accurate enough.

Acknowledgments

The work reported was supported in part by the National Science Foundation through Grant CMMI-0856155 and by the University of Texas at Austin. This support is acknowledged with thanks. Thanks also go to Hexcel Corporation for providing the honeycomb analyzed. The literature on the subject is so vast that makes a more complete citation of related references impractical. Instead, the authors have chosen to cite papers that they found useful in their work.

References

Aktay, L., Johnson, A.F., Kröplin, B.-H., 2008. Numerical modeling of honeycomb core crush behavior. Eng. Fracture Mech. 75, 2616–2630.

Allen, H.G., 1969. Analysis and Design of Structural Sandwich Panels. Pergamon Press.

Bardi, F.C., Yun, H.D., Kyriakides, S., 2003. On the axisymmetric progressive crushing of circular tubes under axial compression. Int. J. Solids Struct. 40, 3137–3155.

Chen, Y., Zhang, Z.-Y., Wang, Y., Hua, H., 2009. Crush dynamics of square honeycomb thin rubber wall. Thin-Walled Struct. 47, 1447–1456.

Floccari, J.F., 2008. On the crushing of honeycomb under combined compression and shear. M.S. Thesis, Engineering Mechanics, The University of Texas at Austin.

Geymonat, G., Müller, S., Triantafyllidis, N., 1993. Homogenization of nonlinearly elastic materials, microscopic bifurcation and macroscopic loss of rank-one convexity. Arch. Rat. Mech. Anal. 122, 231–290.

Gibson, L.J., Ashby, M.F., 1997. Cellular Solids: Structure and Properties, 2nd Ed. Cambridge University Press.

Gibson, LJ., Ashby, M.F., Schajer, G.S., Robertson, C.I., 1982. The mechanics of two-dimensional cellular materials. Proc. Roy. Soc. London A 382, 43–59.

Goldsmith, W., Sackman, J.L., 1992. An experimental study of energy absorption in impact of sandwich plates. Int. J. Impact Eng. 12, 241–262.

Gong, L., Kyriakides, S., Triantafyllidis, N., 2005. On the stability of Kelvin cell foams under compressive loads. J. Mech. Phys. Solids 53, 771–794.

Grediac, M., 1993. A finite element study of the transverse shear in honeycomb. Int. J. Solids Struct. 30, 1777–1788.

Hexcel 2010. Honeycomb attributes and properties. <http://www.hexcel.com/>.

Kelsey, S., Gellanty, R.A., Clark, B.W., 1958. The shear modulus of foil honeycomb core. Aircraft Eng. 30, 294–302.

Klintworth, J.W., Stronge, W.J., 1988. Elasto-plastic yield limits and deformation laws for transversely crushed honeycombs. Int. J. Mech. Sci. 30, 273–292.

Marshall, A., 1982. Sandwich Construction. In: Lubin, G. (Ed.), Handbook of Composites. Van Nostrand Reinhold Comp.

McFarland Jr., R.K., 1963. Hexagonal cell structures under post-buckling axial load. AIAA J. 1, 1380–1385.

McFarland Jr., R.K. 1964. The development of metal honeycomb energy-absorbing elements. Technical Report No. 32-639. Jet Propulsion Laboratory, California Institute of Technology.

Mohr, D., Doyoyo, M., 2003. Nucleation and propagation of plastic collapse bands in aluminum honeycomb. J. Appl. Phys. 94, 2262–2270.

Mohr, D., Doyoyo, M., 2004a. Deformation-induced folding systems in thin-walled monolithic hexagonal metallic honeycomb. Int. J. Solids Struct. 41, 3353–3377.

Mohr, D., Doyoyo, M., 2004b. Experimental investigation on the plasticity of hexagonal aluminum honeycomb under multiaxial loading. J. Appl. Mech. 71, 375–385.

Papka, S.D., Kyriakides, S., 1994. In-plane compressive response and crushing of honeycombs. J. Mech. Phys. Solids 42, 1499–1532.

Papka, S.D., Kyriakides, S., 1998. Experiments and full-scale numerical simulations of in-plane crushing of a honeycomb. Acta Materialia 46, 2765–2776.

Penzien, J., Didriksson, T., 1964. Effective shear modulus of honeycomb cellular structure. AIAA J. 2, 531–535.

Triantafyllidis, N., Schraad, M., 1998. Onset of failure in aluminum honeycombs under general in-plane loading. J. Mech. Phys. Solids 46, 1089–1124.

Wierzbicki, T., 1983. Crushing analysis of metal honeycomb. Int. J. Impact Eng. 1, 157–174.

Wierzbicki, T., Abramowicz, W., 1983. On the crushing mechanics of thin-walled structures. J. Appl. Mech. 50, 727–732.

Wierzbicki, T., Bhat, S.U., Abramovicz, W., Brodkin, D., 1992. Alexander revisited – a two folding elements model of progressive crushing of tubes. Int. J. Solids Struct. 29, 3269–3288.

Yamashita, M., Gotoh, M., 2005. Impact behavior of honeycomb structures with various cell specifications-numerical simulation and experiment. Int. J. Impact Eng. 32, 618–630.

Zhang, J., Ashby, M.F., 1992. The out-of-plane properties of honeycombs. Int. J. Mech. Sci. 34, 475–489.

Zhao, H., Gary, G., 1998. Crushing behaviour of aluminium honeycombs under impact loading. Int. J. Impact Eng. 21, 827–836.